International Journal of Nanomedicine

Dovepress
Taylor & Francis Group

Open Access Full Text Article

ORIGINAL RESEARCH

Spatholobus suberectus Stem-Derived Extracellular Vesicle-Like Particles Attenuate Glucocorticoid-Induced Osteoporosis via NRF2/HO-1 Signaling

Guangmou Chen[1,*], Hongqiang Li[1,2,*], Rihao Chen[1,2,*], Yuan Yao[2], Guan Lian[2], Liping Bai[2], Haosen Chen[1], Chong Zhang[3], Guanghua Chen[1]

[1]Orthopedic Center, Affiliated Hospital of Guangdong Medical University, Zhanjiang, Guangdong, People's Republic of China; [2]The First School of Clinical Medicine, Affiliated Hospital of Guangdong Medical University, Zhanjiang, Guangdong, People's Republic of China; [3]Zhanjiang Institute of Clinical Medicine, Central People's Hospital of Zhanjiang, Guangdong Medical University, Zhanjiang, Guangdong, People's Republic of China

*These authors contributed equally to this work

Correspondence: Guanghua Chen; Chong Zhang, Email chenguanghua@gdmu.edu.cn; zhangchong1992@126.com

Purpose: Glucocorticoid-induced osteoporosis (GIOP) is characterized by impaired osteoblast function and disrupted bone homeostasis during prolonged glucocorticoid exposure. This study investigated whether *Spatholobus suberectus* stem-derived extracellular vesicle-like particles (SS-EVLP) could attenuate glucocorticoid-induced osteogenic impairment and explored the potential involvement of NRF2/HO-1 signaling.

Methods: SS-EVLP were isolated by ultracentrifugation and characterized by transmission electron microscopy, nanoparticle tracking analysis, and Fourier-transform infrared spectroscopy. Cellular uptake was evaluated using PKH26 labeling. In vitro, MC3T3-E1 pre-osteoblastic cells were exposed to dexamethasone (DEX) and treated with SS-EVLP. Cell viability, apoptosis, alkaline phosphatase (ALP) activity, mineralization, and protein expression were assessed by CCK-8 assay, flow cytometry, staining assays, immunofluorescence, and Western blotting. In vivo, the effects of SS-EVLP were examined in a prednisolone-induced zebrafish model by analyzing particle distribution, skeletal mineralization, osteoblast-associated signals, ALP activity, and osteogenic- and antioxidant-related gene expression.

Results: SS-EVLP exhibited vesicle-like spherical morphology and were mainly distributed between approximately 100 and 200 nm, with a major peak at 146 nm. SS-EVLP were efficiently taken up by MC3T3-E1 cells and showed low cytotoxicity. In DEX-treated cells, SS-EVLP restored cell viability, reduced apoptosis, and partially recovered ALP staining and mineralized nodule formation. The reduced expression of RUNX2, SP7, HO-1, and NRF2 in DEX-treated cells was partially restored by SS-EVLP, accompanied by increased nuclear NRF2 signal. In zebrafish, SS-EVLP were detectable in vivo after microinjection, attenuated prednisolone-induced skeletal defects, restored ALP activity, and increased the expression of *runx2a, sp7, nrf2, ho-1, gclc, gstp*, and *nqo1*.

Conclusion: SS-EVLP attenuated glucocorticoid-induced osteogenic impairment in vitro and in vivo, at least partly through NRF2/HO-1 signaling. These findings support the potential of SS-EVLP as a plant-derived nanovesicle candidate for GIOP intervention.

Keywords: bone loss, pre-osteoblasts, antioxidant response, zebrafish model, herbal nanovesicles

Introduction

Osteoporosis is a metabolic skeletal disorder characterized by diminished bone mass and compromised microarchitecture, leading to increased bone fragility and a heightened risk of fractures.[1] Globally, this condition affects over 200 million individuals, with postmenopausal women being the most vulnerable demographic.[2] In addition to adversely affecting quality of life, osteoporosis imposes a significant economic burden on healthcare systems. In the United States, the total medical expenditure for osteoporotic patients surpasses that of non-osteoporotic individuals by approximately

https://doi.org/10.2147/IJN.S585928
Received: 2 December 2025
Accepted: 3 April 2026
Published: 11 April 2026

$8572.15.[3] GIOP emerges as a secondary form of the disorder, primarily due to prolonged glucocorticoid therapy, particularly with dexamethasone. Evidence indicates that glucocorticoids such as dexamethasone induce oxidative stress, impair antioxidant defenses, and suppress osteogenic differentiation programs, thereby contributing to bone loss.[4] Current treatments for GIOP, such as bisphosphonates, selective estrogen receptor modulators (SERMs), and parathyroid hormone (PTH) analogs,[5] are constrained by side effects, limited efficacy, and poor patient adherence.[6] Consequently, there is a pressing need for the development of safer and more effective therapeutic options.

Plant-derived extracellular vesicle-like particles (EVLP) are nanoscale lipid bilayer vesicles released by plant cells that can mediate inter-kingdom communication by transferring bioactive cargos (eg, small RNAs, proteins, and lipids) to recipient cells[7] Compared with mammalian cell–derived exosomes, plant-derived EVLP offer practical advantages for translational exploration, including broad availability, low immunogenicity, favorable biocompatibility, and scalable production potential. Increasing evidence indicates that plant-derived EVLP can modulate oxidative stress and inflammatory signaling, which are key pathological drivers of glucocorticoid-related bone loss.[8]

Spatholobus suberectus stem (Ji Xue Teng), a traditional Chinese medicinal herb, possesses antioxidant and anti-inflammatory properties that are closely associated with bone metabolic regulation.[9,10] Based on these characteristics, we hypothesized that extracellular vesicle-like particles derived from *S. suberectus* stem (SS-EVLP) may alleviate glucocorticoid-induced osteoporosis by attenuating oxidative stress and restoring osteogenic differentiation.

In this study, SS-EVLP were isolated and characterized, and their protective effects were examined in dexamethasone-injured MC3T3-E1 osteoblastic cells and a prednisolone-induced zebrafish model of glucocorticoid-induced osteoporosis. The results indicate that SS-EVLP alleviate glucocorticoid-induced osteogenic impairment and are associated with activation of antioxidant responses, potentially involving NRF2/HO-1 signaling.

Materials and Methods

Reagents and Materials

The medicinal herb *Spatholobus suberectus* stem was purchased from Guangdong Provincial Traditional Chinese Medicine Decoction Pieces Co., Ltd. (Guangzhou, China; Batch No. 231201). Cell Counting Kit-8 (CCK-8) and Annexin V-FITC/PI apoptosis detection kits were purchased from Beyotime (Shanghai, China). The fluorescent dyes PKH26 and DiO were obtained from Sigma-Aldrich (St. Louis, MO, USA). Antibodies against RUNX2, SP7, NRF2, HO-1, GAPDH and β-actin were purchased from Proteintech (Wuhan, China). Nrf2-IN-1, a pharmacological inhibitor of NRF2, was obtained from MedChemExpress (MCE; Monmouth Junction, NJ, USA). AB wild-type zebrafish and Tg(sp7:eGFP) transgenic zebrafish were obtained from the National Zebrafish Resource Center (Wuhan, China).

Isolation and Characterization of Spatholobus suberectus Stem-Derived Extracellular Vesicle-Like Particles

Fresh *Spatholobus suberectus* stem tissue was finely minced, washed twice with distilled water, and homogenized for 3 s using a tissue grinder. The homogenized tissue fragments were then immersed in distilled water and incubated at 37 °C for 20 h. The supernatant was collected and centrifuged at 4000 × g for 30 min to remove tissue debris, followed by centrifugation at 10,000 × g for 30 min to further eliminate impurities. The resulting supernatant was subjected to ultracentrifugation at 100,000 × g for 70 min to pellet *S. suberectus* stem-derived extracellular vesicle-like particles (SS-EVLP). The pellet was resuspended in phosphate-buffered saline (PBS; 1×, pH 7.4; Gibco, USA) and washed again by ultracentrifugation to obtain crude SS-EVLP. Additional PBS washing and repeated ultracentrifugation were performed to reduce contamination by soluble proteins.

The total protein concentration of SS-EVLP was determined using a bicinchoninic acid (BCA) protein assay kit (Beyotime, China). The assay was performed directly on the SS-EVLP suspension, and protein concentrations were calculated using a bovine serum albumin (BSA) standard curve. The morphology of SS-EVLP was examined by transmission electron microscopy (TEM), whereas particle size distribution was measured by nanoparticle tracking analysis (NTA). Particle-associated signal distribution was further evaluated by flow cytometry, and molecular

composition was characterized by Fourier-transform infrared (FTIR) spectroscopy over a spectral range of 400–4000 cm^{-1}, with prunetin (B30453, Yuanye Bio-Technology, Shanghai, China) used as a reference control.

Cell Culture and Experimental Design

MC3T3-E1 murine pre-osteoblastic cells were purchased from Wuhan Procell Life Science & Technology Co., Ltd. (Wuhan, China). Cells were cultured in alpha minimum essential medium (α-MEM) supplemented with 10% fetal bovine serum and 1% penicillin-streptomycin at 37 °C in a humidified incubator with 5% CO_2. Cells were passaged at a ratio of 1:3.

To establish the glucocorticoid-induced injury model, MC3T3-E1 murine pre-osteoblastic cells were exposed to dexamethasone (DEX) at concentrations ranging from 0.1 to 500 μM for 24 or 48 h. Based on preliminary dose-response experiments, 100 μM DEX was selected for subsequent experiments. To assess the effects of SS-EVLP alone, cells were treated with SS-EVLP at 0, 20, 40, 60, or 80 μg/mL for 24 or 48 h. For rescue dose screening, DEX-treated cells were co-incubated with SS-EVLP at 20, 40, 60, 80, or 100 μg/mL for 24 or 48 h. Based on the rescue effects on cell viability, 60 μg/mL SS-EVLP was selected for subsequent experiments. Unless otherwise indicated, cells were assigned to the following groups: Control, DEX (100 μM), DEX + SS-EVLP (60 μg/mL), and SS-EVLP (60 μg/mL).

Cell Viability Assay

Cells were seeded into 96-well plates at a density of 2000 cells per well and treated as indicated above. After treatment, 10 μL of CCK-8 solution was added to each well, and the cells were incubated for 1 h. The absorbance at 450 nm was measured using an Infinite® 200 PRO microplate reader (Tecan, Männedorf, Switzerland).

Assessment of ALP Activity and Alizarin Red S Staining

For alkaline phosphatase (ALP) staining, cells were fixed with 4% paraformaldehyde for 15 min, rinsed with PBS, and incubated with BCIP/NBT working solution (Beyotime, Shanghai, China) at 37 °C for 30 min. The reaction was terminated by washing with distilled water, and images were captured under a light microscope. For Alizarin Red S staining, cells were fixed with 4% paraformaldehyde, washed with PBS, and stained with 0.1% Alizarin Red S solution for 30 min at room temperature. After washing thoroughly with distilled water to remove excess dye, images were captured under a light microscope. Quantification of ALP staining intensity and Alizarin Red S-positive mineralized areas was performed using ImageJ software.

Apoptosis Analysis by Flow Cytometry

After treatment, cells were collected, washed twice with cold PBS, and stained with Annexin V-FITC/PI according to the manufacturer's instructions. After incubation for 15 min at room temperature in the dark, samples were analyzed using a BD FACSAria II flow cytometer, and the percentages of apoptotic cells were quantified with FlowJo software.

Fluorescence Imaging of NRF2 Localization and SS-EVLP Uptake

For immunofluorescence analysis of NRF2 localization, cells were fixed, permeabilized, blocked, and incubated sequentially with an anti-NRF2 primary antibody and an appropriate fluorescent secondary antibody, followed by DAPI counterstaining. NRF2 localization was observed by confocal microscopy.

For uptake analysis, SS-EVLP were labeled with PKH26 and co-incubated with MC3T3-E1 cells for 24 h. After fixation, cells were stained with phalloidin to visualize the cytoskeleton and with DAPI to label nuclei. Intracellular uptake of PKH26-labeled SS-EVLP was assessed by confocal microscopy.

Fluorescent Labeling of SS-EVLP

For fluorescence labeling, SS-EVLP were resuspended in Diluent C (Sigma-Aldrich), incubated with PKH26 or DiO according to the manufacturer's instructions for 5 min at room temperature, and then ultracentrifuged at 100,000 × g for 70 min. The pellet was washed with PBS to remove unbound dye and finally resuspended in PBS for subsequent cell or zebrafish experiments.

Western Blotting

Total protein was extracted using RIPA lysis buffer. Protein samples were quantified, separated by 8–12% SDS-PAGE, and transferred onto PVDF membranes. After blocking, the membranes were incubated with primary antibodies followed by HRP-conjugated secondary antibodies. Protein bands were visualized using an enhanced chemiluminescence (ECL) substrate, and densitometric analysis was performed using Image Lab software. β-actin was used as the internal control. Primary antibodies against NRF2, HO-1, RUNX2, SP7, GAPDH and β-actin were used at the following dilutions: NRF2, 1:5000; HO-1, 1:20000; RUNX2, 1:500; SP7, 1:1000; GAPDH, 1:20000 and β-actin, 1:8000. An HRP-conjugated goat anti-rabbit IgG secondary antibody was used at a dilution of 1:5000.

Quantitative Real-Time PCR

Total RNA was extracted using TRIzol reagent and reverse-transcribed into complementary DNA (cDNA) using the PrimeScript™ RT Reagent Kit with gDNA Eraser (RR047A; Takara, Japan). Quantitative real-time PCR (qPCR) was performed using PerfectStart® Green qPCR SuperMix (AQ601; TransGen Biotech, Beijing, China) on a LightCycler® 480 Instrument II (Roche, Basel, Switzerland). Primer sequences are listed in Table 1. *β-actin* was used as the internal housekeeping gene for normalization, and relative gene expression was calculated using the $2^{-\Delta\Delta Ct}$ method.

Zebrafish Model of Glucocorticoid-Induced Osteoporosis

Wild-type AB zebrafish and Tg(sp7:eGFP) transgenic zebrafish were maintained at 28.5 °C under a 14 h light/10 h dark cycle. Embryos were exposed to prednisolone (PDN; 25 μM) from 2 to 9 days post-fertilization (dpf) to establish a zebrafish model of glucocorticoid-induced osteoporosis.[11,12] The culture medium was refreshed daily by replacing half of the embryo medium. For SS-EVLP treatment, PDN-exposed larvae were treated with SS-EVLP at concentrations of 10, 20, or 40 μg/mL. Unless otherwise indicated, 20 μg/mL SS-EVLP was used in subsequent experiments.

In vivo Distribution of SS-EVLP in Zebrafish

DiO-labeled SS-EVLP were prepared as described above. Zebrafish embryos were anesthetized and microinjected with DiO-labeled SS-EVLP (500 ng/μL, 2 nL per embryo) into the pericardial cavity using a PLI-100A microinjection system (Harvard Apparatus, Holliston, MA, USA). Confocal fluorescence imaging was performed at 1 and 3 days post-injection to assess the in vivo distribution of SS-EVLP.

Functional Assessment of Osteogenesis in Zebrafish

At 9 dpf, zebrafish larvae were collected for the evaluation of skeletal mineralization and alkaline phosphatase (ALP) activity. For mineralization analysis, larvae were fixed in 4% paraformaldehyde, stained with 0.1% Alizarin Red S for 30 min, rinsed thoroughly with distilled water, and imaged under a stereomicroscope. ALP activity was measured using

Table 1 Primer Sequences for Quantitative Real-Time PCR

Genes	Forward (5′-3′)	Reverse (5′-3′)
runx2a	ACGGTAATGGCTGGAAATGA	GTCCGTCCACTGTGACCTTT
sp7	TCCAGACCTCCAGTGTTTCC	ATGGACATCCCACCAAGAAG
nrf2	GCACACCGCTCACACACACACC	CCGACTCAGCCGGCTCTGTTAG
gstp1	CGACTGAAAGCCACCTGTGTC	CTGTCGTTTTTGCCATATGCAGC
nqo1	TTCAGCTACTGCGGAGGAT	TCTGGTTGTTTGGTGGGAG
gclc	AACCGACACCCAAAGATTCAGCACT	CCATCATCCTCTGGAAACACCTCC
ho-1	ACAGAAACGCAGACCACCC	CTCCAGGAAACGAGAAGAATAAA
β-actin	CGAGCTGTCTTCCCATCCA	TCACCAACGTAGCTGTCTTTCTG

a colorimetric assay kit according to the manufacturer's instructions (Nanjing Jiancheng Bioengineering Institute, Nanjing, China), with 30 embryos pooled per sample. Quantification of mineralized areas was performed using ImageJ software.

Whole-Mount in situ Hybridization

Whole-mount in situ hybridization for *col10a1a* was performed on zebrafish larvae as previously described.[13,14]

Statistical Analysis

Data are presented as mean ± SD. Statistical analyses were performed using GraphPad Prism 9.0 software (GraphPad Software, San Diego, CA, USA). Comparisons among multiple groups were performed using one-way ANOVA followed by Dunnett's multiple-comparisons test.

Results

Physicochemical Characterization and Cellular Uptake of SS-EVLP

Transmission electron microscopy (TEM) showed that SS-EVLP exhibited vesicle-like spherical morphology (Figure 1a). Nanoparticle tracking analysis (NTA) showed that SS-EVLP were predominantly distributed between approximately 100 and 200 nm, with a major peak at 146 nm (Figure 1b). Fourier-transform infrared spectroscopy (FTIR) was then performed to characterize their chemical composition. Compared with the spectrum of prunetin used as a reference compound (Figure 1c), the SS-EVLP spectrum displayed distinct absorption peaks, indicating the presence of characteristic molecular components in the isolated particles (Figure 1d). In addition, PKH26-labeled SS-EVLP were detected in MC3T3-E1 pre-osteoblastic cells after incubation, whereas little signal was observed in the control group, indicating efficient uptake of SS-EVLP by these cells (Figure 1e).

SS-EVLP Attenuate DEX-Induced Loss of Viability and Apoptosis in Osteoblastic Cells

CCK-8 assays were performed to evaluate the effects of SS-EVLP and dexamethasone (DEX) on the viability of MC3T3-E1 cells. At 24 h, treatment with 20–80 μg/mL SS-EVLP did not reduce cell viability and instead resulted in a modest increase relative to the untreated control (Figure 2a). A similar trend was observed at 48 h, although the increase was less evident at the highest concentration (Figure 2d), indicating low cytotoxicity of SS-EVLP within the tested concentration range. By contrast, DEX reduced MC3T3-E1 cell viability in a concentration-dependent manner at both 24 h and 48 h over the tested range of 0.1–500 μM (Figure 2b and e). Cell viability progressively declined with increasing DEX concentration, and the reduction became more pronounced at concentrations above 100 μM. Therefore, 100 μM DEX was selected for subsequent rescue experiments to ensure effective model induction while preserving sufficient cell survival. Under 100 μM DEX exposure, co-treatment with SS-EVLP significantly restored cell viability at both time points, with the strongest protective effect observed at 60 μg/mL (Figure 2c and f).

To further determine whether SS-EVLP affected DEX-induced apoptosis, Annexin V-FITC/PI staining was analyzed by flow cytometry. DEX markedly increased the proportion of apoptotic cells compared with the control group, whereas co-treatment with SS-EVLP substantially reduced apoptosis relative to the DEX group (Figure 2g and h). These findings support a protective effect of SS-EVLP against DEX-induced apoptosis in MC3T3-E1 cells.

SS-EVLP Promote Osteogenic Differentiation and are Associated with Changes in NRF2/HO-1 Signaling

To assess osteogenic differentiation under different treatment conditions, ALP staining and Alizarin Red S staining were performed. Compared with the control group, DEX treatment markedly reduced ALP staining intensity and mineralized nodule formation, whereas SS-EVLP treatment partially restored both ALP staining and Alizarin Red S staining in DEX-treated cells (Figure 3a and b).

We next assessed the expression of osteogenic and antioxidant-related proteins. Compared with the control group, the protein levels of RUNX2, SP7, HO-1, and NRF2 were reduced in the DEX-treated group, whereas partial restoration of

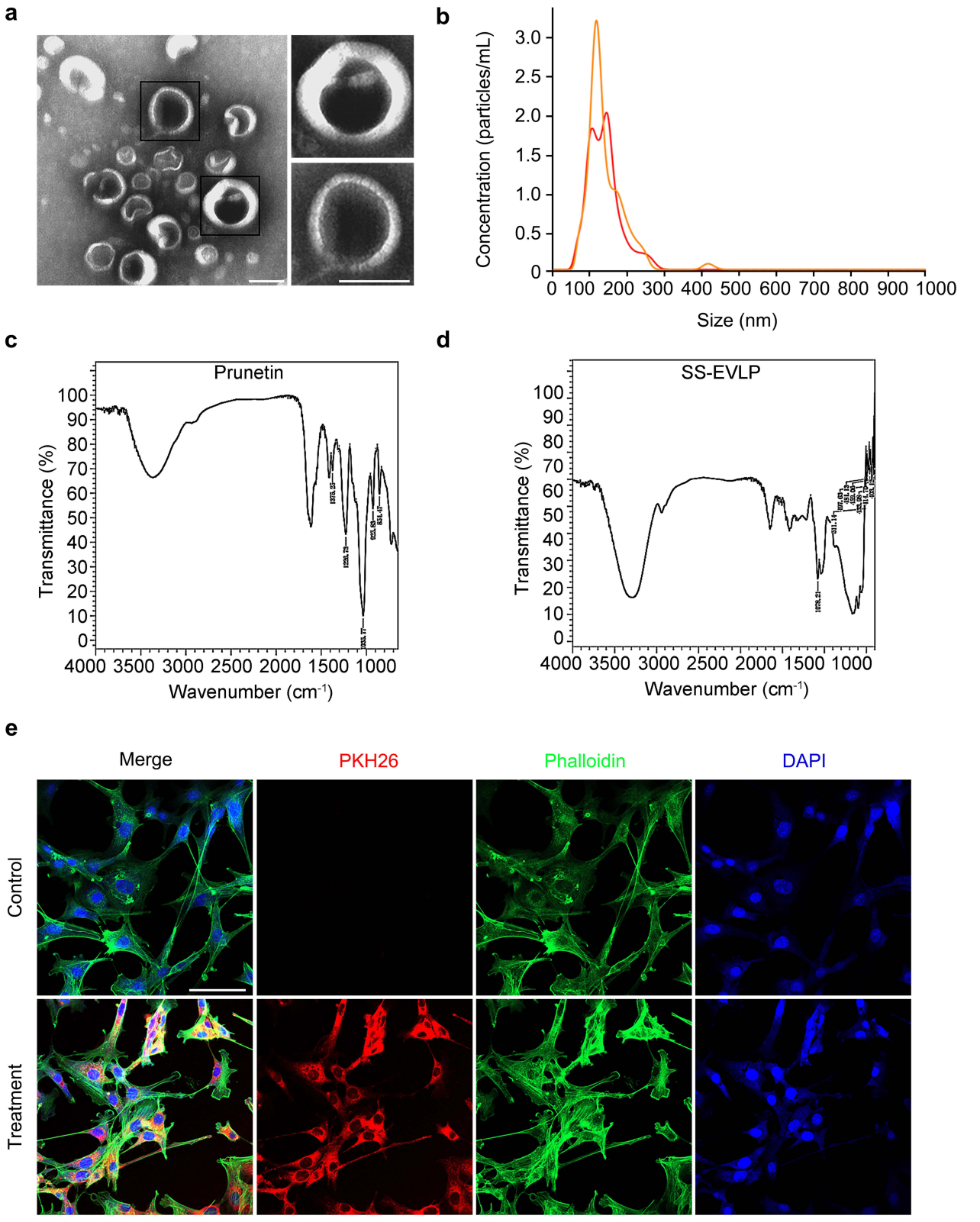

Figure 1 Physicochemical characterization of SS-EVLP. (**a**) Transmission electron microscopy showed that SS-EVLP exhibited vesicle-like spherical morphology. Representative enlarged views are shown on the right. Scale bar: 100 nm. (**b**) Nanoparticle tracking analysis (NTA) showed the size distribution of SS-EVLP. (**c**) Fourier-transform infrared spectroscopy (FTIR) spectrum of the reference compound prunetin. (**d**) Fourier-transform infrared spectroscopy (FTIR) spectrum of SS-EVLP, showing characteristic absorption peaks. (**e**) PKH26 fluorescence labeling demonstrated cellular uptake of SS-EVLP by MC3T3-E1 cells. Red, PKH26-labeled SS-EVLP; green, phalloidin; blue, DAPI. Scale bar: 100 μm.

https://doi.org/10.2147/IJN.S585928

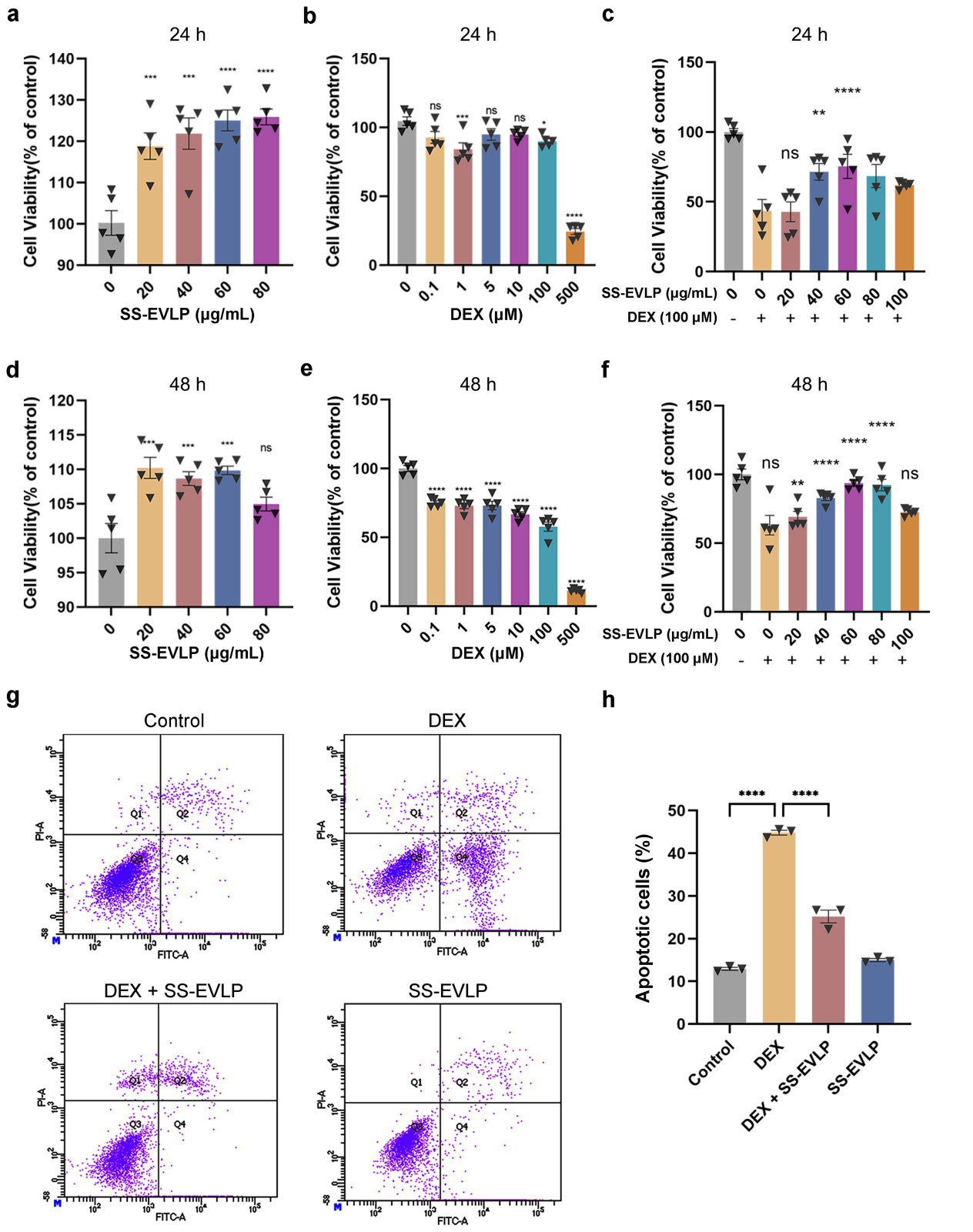

Figure 2 SS-EVLP attenuates dexamethasone-induced loss of viability and apoptosis in MC3T3-E1 cells. (**a** and **d**) Effects of different concentrations of SS-EVLP on MC3T3-E1 cell viability at 24 and 48 h, respectively. (**b** and **e**) Effects of different concentrations of dexamethasone (DEX) on MC3T3-E1 cell viability at 24 and 48 h, respectively. (**c** and **f**) SS-EVLP-mediated restoration of cell viability in MC3T3-E1 cells exposed to 100 μM DEX at 24 and 48 h, respectively. (**g**) Representative flow cytometric plots of Annexin V-FITC/PI double staining in the indicated groups. (**h**) Quantification of apoptotic cells. Data are presented as mean ± SD. Statistical significance was determined by one-way ANOVA followed by Dunnett's multiple-comparisons test. *$P < 0.05$; **$P < 0.01$; ***$P < 0.001$; ****$P < 0.0001$.
Abbreviation: ns, not significant.

https://doi.org/10.2147/IJN.S585928

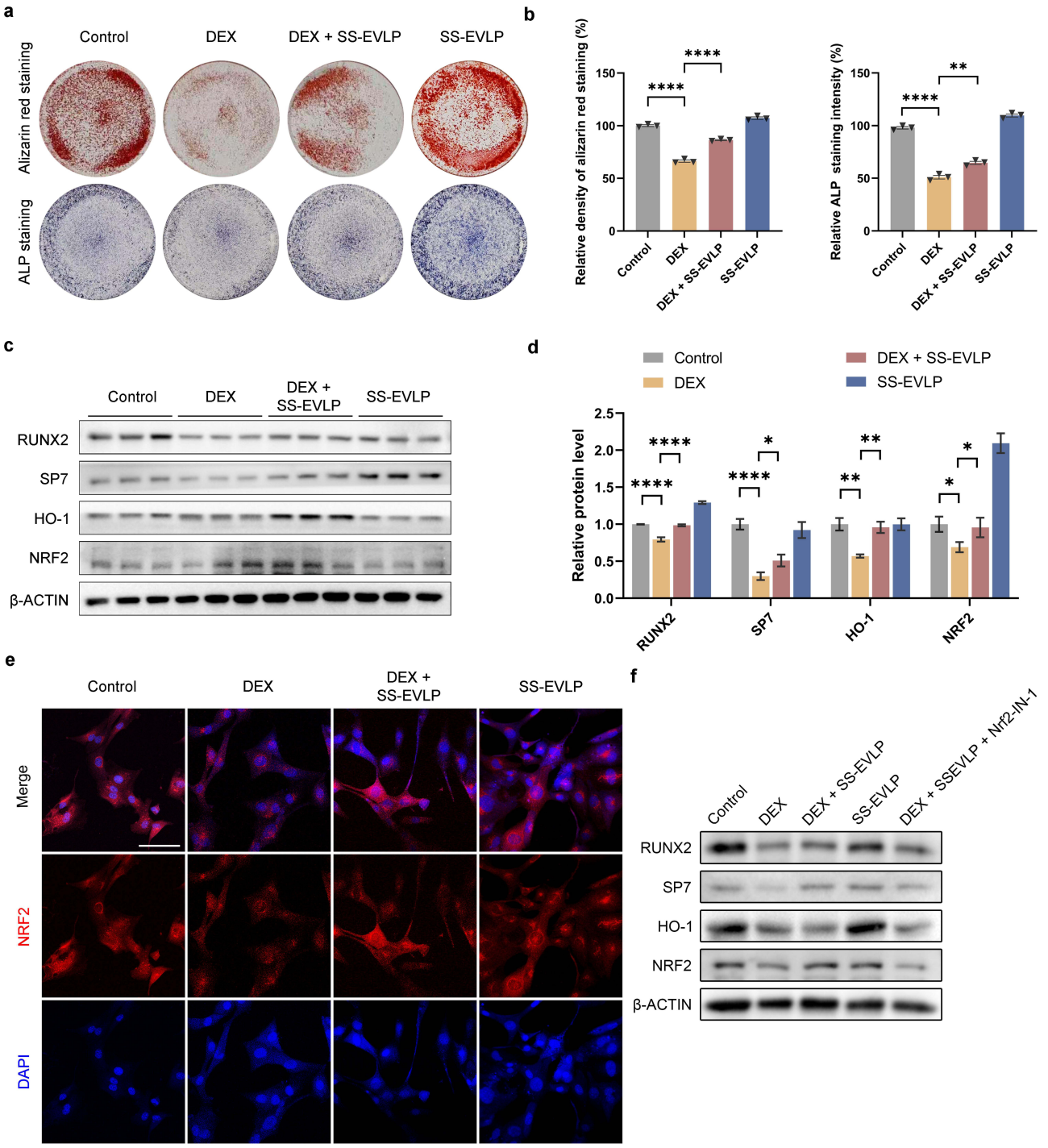

Figure 3 SS-EVLP activates Nrf2/HO-1 signaling and enhances osteogenic differentiation in MC3T3-E1 cells. (**a**) Representative images of Alizarin Red S staining and ALP staining in the Control, DEX, DEX + SS-EVLP, and SS-EVLP groups. (**b**) Quantification of Alizarin Red S staining density and ALP staining intensity. (**c**) Representative Western blot images of RUNX2, SP7, HO-1, and NRF2 protein expression in the indicated groups. β-actin was used as the loading control. (**d**) Densitometric quantification of the protein bands shown in (**c**). (**e**) Immunofluorescence staining showing NRF2 localization in MC3T3-E1 cells under the indicated treatments. NRF2 is shown in red and nuclei are stained with DAPI (blue). Scale bar: 100 μm. (**f**) Representative Western blot analysis performed in the presence of the Nrf2 inhibitor Nrf2-IN-1. Cells were treated as indicated, and the protein levels of RUNX2, SP7, HO-1, and NRF2 were detected. β-actin was used as the loading control. Data are presented as mean ± SD. Statistical significance in (**b** and **d**) was determined by one-way ANOVA followed by Dunnett's multiple-comparisons test. *$P < 0.05$; **$P < 0.01$; ****$P < 0.0001$.
Abbreviation: ns, not significant.

https://doi.org/10.2147/IJN.S585928

these proteins was observed in the DEX + SS-EVLP group (Figure 3c). Densitometric analysis showed a similar trend (Figure 3d). Immunofluorescence staining further showed stronger nuclear NRF2 signal in the DEX + SS-EVLP group than in the DEX group (Figure 3e).

To further examine the role of NRF2 signaling in osteogenic marker expression, cells were treated with the NRF2 inhibitor Nrf2-IN-1. Under these conditions, the SS-EVLP-associated increases in RUNX2, SP7, HO-1, and NRF2 were attenuated (Figure 3f). These results suggest that NRF2 signaling contributes to the regulation of osteogenic marker expression during SS-EVLP treatment under DEX-induced stress.

In vivo Distribution of SS-EVLP in Zebrafish

To examine the in vivo distribution of SS-EVLP, DiO-labeled SS-EVLP were microinjected into Tg(sp7:eGFP) zebrafish and imaged at 1 and 3 days post-injection. Fluorescence signals derived from SS-EVLP were detected in both the trunk and tail regions at 1 day post-injection (Figure 4). Although the signal intensity decreased by 3 days post-injection, fluorescence remained detectable.

SS-EVLP Attenuate Prednisolone-Induced Skeletal Defects in Zebrafish

We next evaluated the effects of SS-EVLP in a prednisolone (PDN)-induced zebrafish model of glucocorticoid-induced osteoporosis. Alizarin Red S staining showed that PDN treatment markedly impaired craniofacial mineralization compared with the control group, whereas SS-EVLP treatment attenuated these defects, with the most evident improvement observed at 20 μg/mL (Figure 5a). In Tg(sp7:eGFP) zebrafish, PDN reduced osteoblast-associated fluorescence, whereas SS-EVLP treatment partially restored this signal (Figure 5b). Whole-mount in situ hybridization further showed that *col10a1a*, an osteogenic marker gene, was downregulated in the PDN group and partially restored after SS-EVLP treatment (Figure 5c). Together, these findings indicate that SS-EVLP attenuate PDN-induced skeletal defects in zebrafish.

SS-EVLP Enhance ALP Activity and Upregulate Osteogenic and Antioxidant-Related Genes in PDN-Treated Zebrafish

To further assess the effects of SS-EVLP in vivo, ALP activity and osteogenic- and antioxidant-related gene expression were examined in zebrafish larvae. PDN exposure significantly reduced ALP activity, whereas SS-EVLP treatment restored ALP levels compared with the PDN group (Figure 6a). qPCR analysis showed that SS-EVLP significantly increased the expression of osteogenic genes, including runx2a and sp7, as well as antioxidant-related genes, including

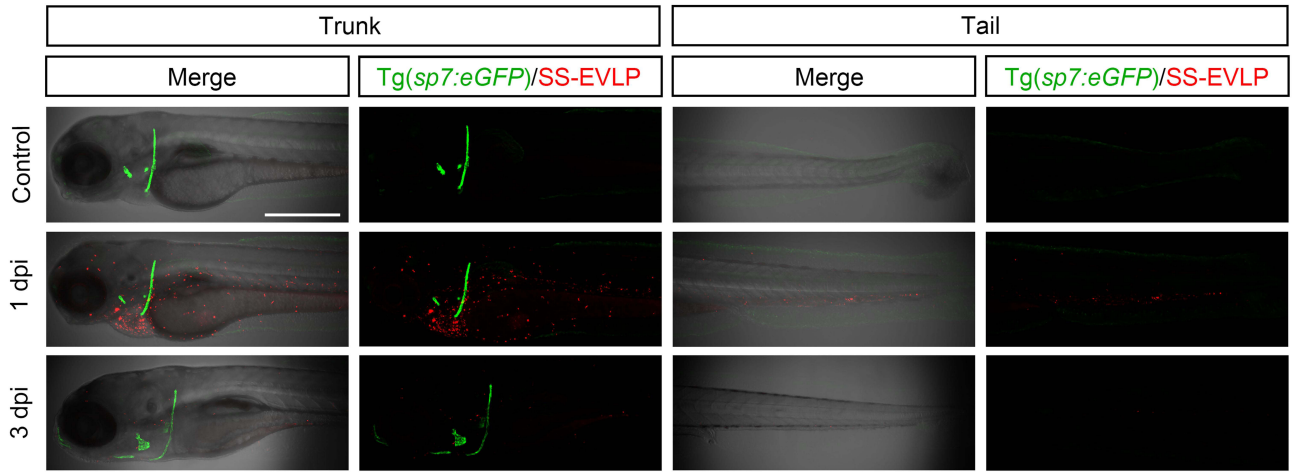

Figure 4 In vivo uptake and distribution of SS-EVLP in zebrafish. Representative fluorescence images showing the in vivo distribution of SS-EVLP in Tg(sp7:eGFP) zebrafish following microinjection of DiO-labeled SS-EVLP. Signals were detected in the trunk and tail regions at 1 and 3 days post-injection, indicating in vivo distribution and persistence of SS-EVLP. Green, Tg(sp7:eGFP); red, DiO-labeled SS-EVLP; merge, overlay of fluorescence and bright-field images. Scale bar: 500 μm.

https://doi.org/10.2147/IJN.S585928

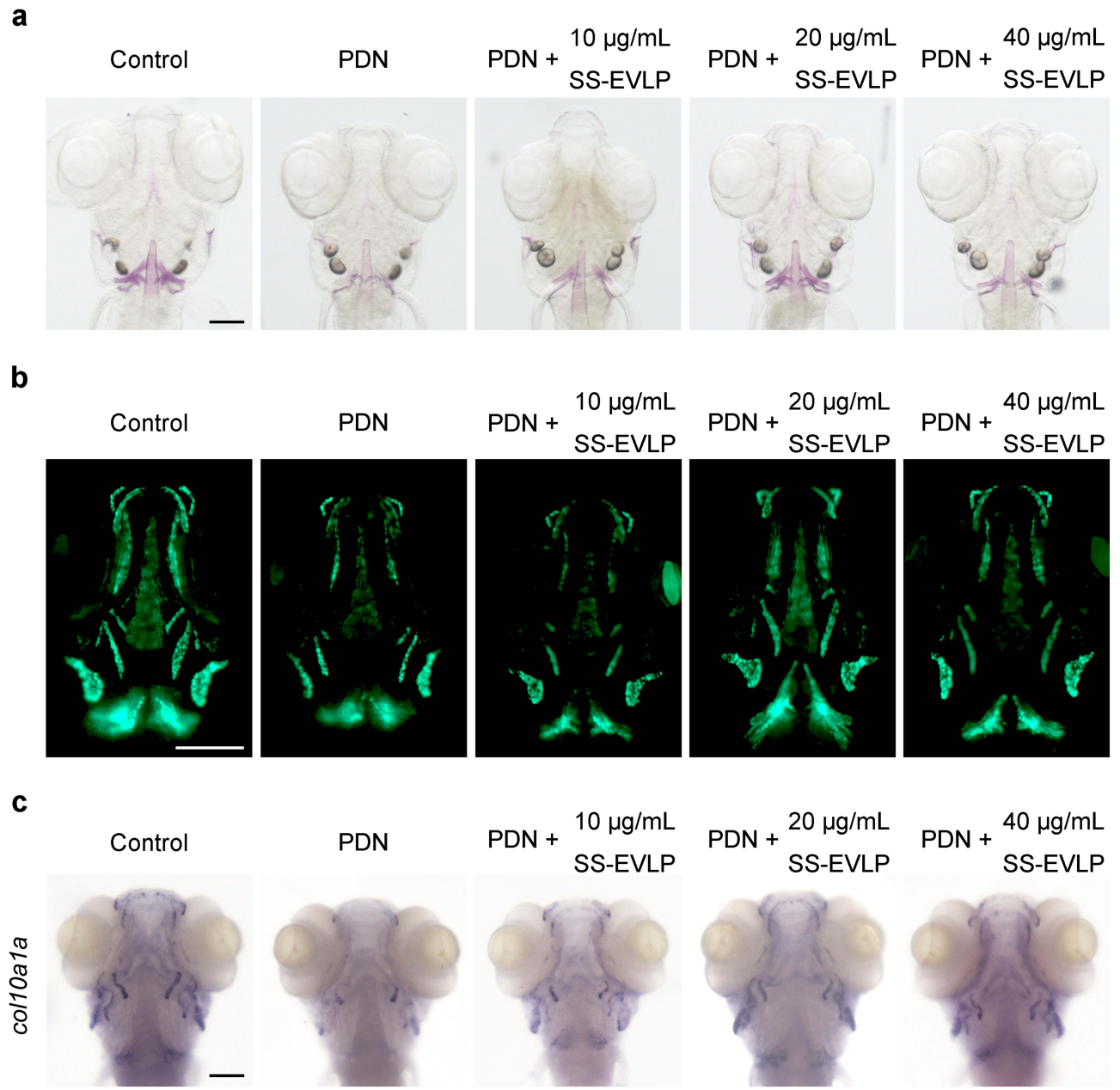

Figure 5 SS-EVLP attenuates prednisolone-induced skeletal defects in zebrafish. (**a**) Representative Alizarin Red S staining images showing craniofacial mineralization in Control, PDN-treated, and PDN + SS-EVLP-treated zebrafish larvae. (**b**) Representative fluorescence images of Tg(sp7:eGFP) zebrafish showing osteoblast-associated fluorescence in the indicated groups. (**c**) Whole-mount in situ hybridization showing the expression pattern of *col10a1a* in zebrafish larvae from different treatment groups. Scale bar: 200 μm.

nrf2, ho-1, gclc, gstp, and *nqo1*, relative to the PDN group (Figure 6b–h). These findings indicate that SS-EVLP treatment is associated with restoration of ALP activity and increased expression of osteogenic- and antioxidant-related genes in PDN-treated zebrafish.

Discussion

This study demonstrates that SS-EVLP exert protective effects against glucocorticoid-induced osteoporosis (GIOP) and provides preliminary mechanistic insight into their action through activation of the NRF2/HO-1 signaling pathway and enhancement of osteogenic gene expression. Both in vitro assays and zebrafish experiments showed that SS-EVLP significantly attenuated dexamethasone-induced osteoblast dysfunction, which was manifested by reduced cell viability,

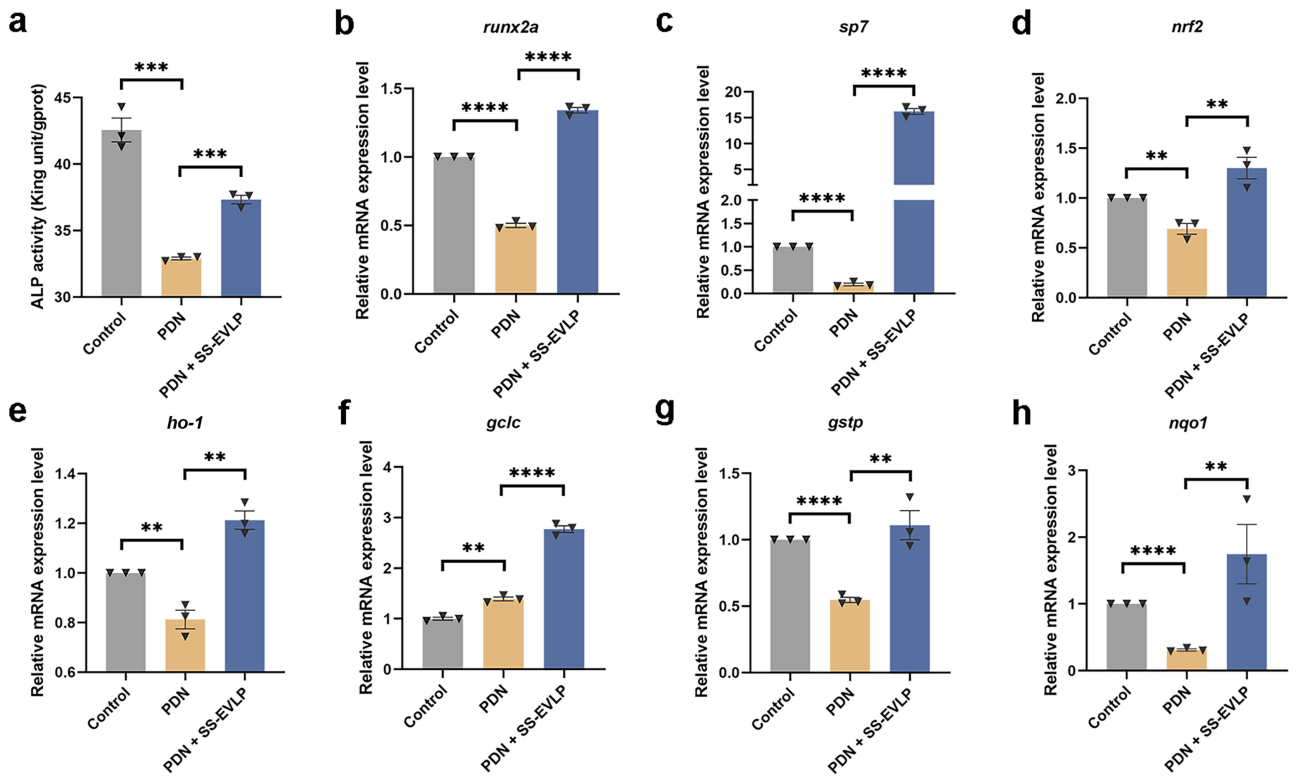

Figure 6 SS-EVLP enhances ALP activity and upregulates osteogenic and antioxidant-related genes in GIOP zebrafish. (**a**) Quantitative analysis of ALP activity in zebrafish larvae from the indicated groups. (**b**–**h**) Relative mRNA expression levels of osteogenic and antioxidant-related genes, including *runx2a, sp7, nrf2, ho-1, gclc, gstp*, and *nqo1*. Data are presented as mean ± SD. Statistical significance was determined by one-way ANOVA followed by Dunnett's multiple-comparisons test. $^{**}P < 0.01$; $^{***}P < 0.001$; $^{****}P < 0.0001$.

impaired differentiation, and increased apoptosis. These findings provide experimental evidence supporting SS-EVLP as a potential therapeutic candidate for osteoporosis and highlight the feasibility of extracellular vesicle-based strategies derived from medicinal plants.

SS-EVLP Mitigates Osteoporotic Damage

Extracellular vesicles have increasingly been recognized as important regulators of bone metabolism. However, most studies to date have focused on vesicles derived from mammalian stem cells or animal cells,[15–17] whereas the therapeutic potential of plant-derived extracellular vesicle-like particles in osteoporosis remains largely unexplored. In the present study, SS-EVLP were evaluated using both dexamethasone-injured MC3T3-E1 osteoblasts and a zebrafish model of glucocorticoid-induced osteoporosis. SS-EVLP markedly reversed dexamethasone-induced osteoblast dysfunction, as reflected by improved cell viability, enhanced mineralized nodule formation, and reduced apoptosis. These findings indicate that SS-EVLP can effectively counteract glucocorticoid-induced impairment of osteoblast function and suggest their potential value as anti-osteoporotic agents.

Extracellular vesicle-based therapeutics have attracted considerable attention because of several intrinsic advantages as biological delivery systems. Their lipid bilayer structure confers excellent biocompatibility and low immunogenicity, thereby reducing the likelihood of immune rejection.[18] Their ability to cross biological barriers may facilitate efficient delivery of therapeutic cargos to target tissues, thereby improving therapeutic efficacy.[19] In addition, extracellular vesicles can efficiently transport diverse biomolecules—including proteins, nucleic acids, and lipids—to recipient cells, enabling multifaceted biological regulation.[20,21] Engineered vesicles have also shown improved cargo loading efficiency and therapeutic stability.[22,23] Although challenges remain regarding large-scale purification and standardization of cargo loading, extracellular vesicles are widely regarded as promising next-generation nanocarriers.[24] In the

https://doi.org/10.2147/IJN.S585928

present study, the successful isolation and biological activity of SS-EVLP provide additional support for the therapeutic potential of plant-derived vesicles in bone-related diseases.

Mechanistic Insights: Nrf2/HO-1 Pathway and Osteogenic Regulation

The protective effects of SS-EVLP appear to be closely associated with activation of the NRF2/HO-1 antioxidant signaling pathway and the stimulation of osteogenic transcriptional programs. The NRF2/HO-1 pathway plays a central role in maintaining cellular redox homeostasis by regulating the expression of antioxidant genes.[25] Activation of this pathway has been shown to alleviate oxidative damage and preserve osteoblast function under glucocorticoid exposure.[26–28] Consistent with these findings, SS-EVLP treatment in the present study significantly increased both mRNA and protein levels of NRF2 and HO-1, accompanied by upregulation of the osteogenic transcription factors RUNX2 and SP7. RUNX2 and Osterix (SP7) are key regulators of osteoblast differentiation. RUNX2 initiates the osteogenic program by inducing SP7 expression and regulating extracellular matrix–related genes in coordination with multiple signaling pathways, including Hedgehog, FGF, Wnt, and PTHrP.[29,30] SP7 subsequently promotes osteoblast maturation and mineralization, playing an indispensable role in both intramembranous and endochondral ossification.[31] The increased expression of RUNX2 and SP7 observed in this study likely contributes to the enhanced osteogenic activity induced by SS-EVLP.

Further evidence for the involvement of this pathway was obtained using the NRF2 inhibitor Nrf2-IN-1. Pharmacological inhibition of NRF2 partially attenuated the SS-EVLP-induced upregulation of RUNX2, SP7, and HO-1, indicating that activation of the NRF2/HO-1 signaling axis is an important component of the observed protective effects.

Extracellular vesicles are known to carry diverse bioactive cargo, including miRNAs and proteins, which can regulate cellular proliferation, differentiation, and apoptosis by targeting specific molecular pathways.[32,33] It is therefore possible that SS-EVLP exert their biological activity through the delivery of regulatory molecules that influence oxidative stress signaling and osteogenic differentiation.

Although SS-EVLP clearly enhanced NRF2/HO-1 signaling in this study, the precise molecular mechanisms responsible for this activation remain unclear. Extracellular vesicle cargo may modulate regulators of NRF2, such as KEAP1, or affect upstream kinases including PKC and MAPK.[34–36] Determining whether specific miRNAs or proteins contained within SS-EVLP directly target the KEAP1–NRF2 axis will require further investigation. Moreover, while our findings demonstrate a strong association between NRF2 activation and osteogenic recovery, additional mechanistic studies—such as genetic knockdown of NRF2 or modulation of HO-1 expression—would be necessary to establish definitive causal relationships.

Advantages and Future Applications of Plant-Derived Extracellular Vesicles

Plant-derived extracellular vesicle-like particles have recently emerged as promising natural nanocarriers because of their low immunogenicity, high biocompatibility, and efficient cellular uptake.[37] These vesicles can transport a wide range of bioactive compounds and may enhance the stability and bioavailability of therapeutic molecules.[38] Previous studies have demonstrated that plant-derived vesicles can exert anti-inflammatory, anti-tumor, and antioxidant effects through modulation of immune responses and intracellular signaling pathways.[39]

Beyond glucocorticoid-induced osteoporosis, the biological characteristics of plant-derived EVLP suggest potential applications in other diseases associated with chronic inflammation and oxidative stress. In particular, inflammatory bone disorders—such as arthritis-related bone erosion, periodontitis-associated alveolar bone loss, and wear particle-induced osteolysis—may represent additional therapeutic targets for vesicle-based interventions.[40–42] Given that oxidative stress and inflammatory signaling are common pathological drivers across multiple skeletal disorders, the therapeutic potential of SS-EVLP may extend beyond GIOP and warrants further investigation in other bone-loss conditions. Nevertheless, further work is required to overcome challenges related to large-scale production, purification standardization, and quality control before clinical translation can be realized.[43] The present findings provide a foundation for future exploration of medicinal plant-derived EVLP as therapeutic agents for bone diseases.

Limitations and Future Directions

Despite the encouraging results, several limitations should be acknowledged. First, the present study relied on in vitro experiments and a zebrafish model, without validation in mammalian systems such as rodents. Given the physiological differences in skeletal biology, metabolism, and pharmacokinetics between zebrafish and mammals, the translational relevance of the findings requires further confirmation.

Second, SS-EVLP were administered to zebrafish through immersion exposure, which differs from potential clinical delivery routes such as systemic administration or local injection. Consequently, the exposure dynamics and effective dosing observed in zebrafish may not directly reflect those in mammalian organisms. Future studies using glucocorticoid-treated rodent models will be necessary to evaluate bone mineral density, histomorphometric parameters, and pharmacokinetic characteristics.

In addition, the specific bioactive components responsible for the therapeutic activity of SS-EVLP remain unidentified. Comprehensive characterization of vesicle cargo through proteomic and miRNA sequencing approaches may help identify key molecules and clarify their intracellular targets, thereby facilitating the rational development of SS-EVLP-based therapies.

Clinical Translation of SS-EVLP

Although our findings provide preclinical evidence that SS-EVLP can protect against glucocorticoid-induced osteogenic impairment, careful evaluation will be required before clinical translation. The concentrations used in this study (60 μg/mL in vitro and 20 μg/mL in zebrafish) were selected based on preliminary toxicity testing and previous studies of plant-derived vesicles but cannot be directly extrapolated to human dosing. Detailed pharmacokinetic, biodistribution, and bioavailability studies in mammalian models will be necessary to determine clinically relevant exposure levels.

Moreover, large-scale isolation, purification, and standardization of SS-EVLP remain important technical challenges. Addressing these issues will be essential for future clinical development. Therefore, while SS-EVLP represent a promising therapeutic strategy, comprehensive preclinical evaluation in mammalian systems will be a critical step toward eventual clinical application.

Conclusion

This study demonstrates that extracellular vesicle-like particles derived from *Spatholobus suberectus* stem (SS-EVLP) exert protective effects against glucocorticoid-induced osteogenic impairment. SS-EVLP significantly improved osteoblast viability, reduced apoptosis, and enhanced osteogenic differentiation in dexamethasone-injured MC3T3-E1 cells, while also alleviating bone mineralization defects in a prednisolone-induced zebrafish model of glucocorticoid-induced osteoporosis. Mechanistically, these protective effects were associated with activation of the NRF2/HO-1 antioxidant signaling pathway and upregulation of key osteogenic transcription factors, including RUNX2 and SP7. Collectively, these findings suggest that SS-EVLP represent a promising natural nanotherapeutic candidate for the prevention or treatment of glucocorticoid-induced osteoporosis. Further studies in mammalian models are warranted to evaluate their pharmacological properties and translational potential.

Abbreviations

ALP, alkaline phosphatase; ARS, Alizarin Red S; BCA, bicinchoninic acid; BSA, bovine serum albumin; CCK-8, Cell Counting Kit-8; DEX, dexamethasone; dpf, days post-fertilization; ECL, enhanced chemiluminescence; EVLP, extracellular vesicle-like particles; FTIR, Fourier-transform infrared spectroscopy; GIOP, glucocorticoid-induced osteoporosis; HO-1, heme oxygenase 1; Nrf2/NRF2, nuclear factor erythroid 2-related factor 2; NTA, nanoparticle tracking analysis; PBS, phosphate-buffered saline; PDN, prednisolone; PFA, paraformaldehyde; PTH, parathyroid hormone; PVDF, polyvinylidene fluoride; qPCR, quantitative real-time polymerase chain reaction; RIPA, radioimmunoprecipitation assay; SERMs, selective estrogen receptor modulators; SS-EVLP, *Spatholobus suberectus* stem-derived extracellular vesicle-like particles; TEM, transmission electron microscopy; TRIzol, total RNA isolation reagent; WISH, whole-mount in situ hybridization.

Data Sharing Statement

The datasets generated and/or analyzed during the current study are available from the corresponding authors (Guanghua Chen and Chong Zhang) upon reasonable request.

Ethical Approval

All animal experiments were performed in accordance with the guidelines for the care and use of laboratory animals and were approved by the Animal Care and Ethics Committee of Central People's Hospital of Zhanjiang (Approval No. DW-2025008).

Acknowledgments

This work was supported by the Guangdong Basic and Applied Basic Research Foundation (2023A1515110960 and 2024A1515010834), the National Natural Science Foundation of China (32400686), the High-Level Talent Scientific Research Initiation Project of the Affiliated Hospital of Guangdong Medical University (GCC2022003), the Clinical and Basic Research Innovation Program of Guangdong Medical University (GDMULCJC2024011), the Guangdong Province Medical Science and Technology Research Fund Project (A2025261) and the Doctoral Startup Fund of Central People's Hospital of Zhanjiang (2022A12).

Author Contributions

GMC, HL, and RC contributed equally to this work. GHC, CZ, and HL conceived and designed the study. GMC, HL, RC, YY, GL, LB, and HC performed the experiments and acquired the data. GMC, HL, RC, CZ, and GHC analyzed and interpreted the data. GMC, HL, and RC drafted the manuscript. GHC, CZ, and HL critically revised the manuscript for important intellectual content and supervised the study. All authors made substantial contributions to the work reported, approved the final version of the manuscript, agreed on the journal to which the article has been submitted, and agreed to be accountable for all aspects of the work, including ensuring that any questions related to the accuracy or integrity of any part of the work are appropriately investigated and resolved.

Disclosure

The authors declare no competing interests.

References

1. De Mattia G, Maffi M, Mazzantini M. Anabolic treatment for osteoporosis and fragility fracture risk: one year in review 2024. *Clin Exp Rheumatol*. 2024;42(7):1311–1316. doi:10.55563/clinexprheumatol/7f52vl
2. Dastmanesh S, Karimi M, Ghahremani L, Seif M, Zare E. A health communication campaign for prevention of osteoporosis in rural elderly women. *BMC Womens Health*. 2023;23(1):124. doi:10.1186/s12905-023-02282-7
3. Masurkar PP, Rege S. Marginal health care expenditures and health-related quality of life burden in patients with osteoporosis in the United States. *J Am Pharm Assoc*. 2025;65(2):102315. doi:10.1016/j.japh.2024.102315
4. Saleh SR, Saleh OM, El-Bessoumy AA, Sheta E, Ghareeb DA, Eweda SM. The therapeutic potential of two Egyptian plant extracts for mitigating dexamethasone-induced osteoporosis in rats: nrf2/HO-1 and RANK/RANKL/OPG signals. *Antioxidants*. 2024;13(1):66. doi:10.3390/antiox13010066
5. Tanaka Y, Soen S, Hirata S, et al. The 2023 Guidelines for the management and treatment of glucocorticoid-induced osteoporosis. *J Bone Miner Metab*. 2024;42(2):143–154. doi:10.1007/s00774-024-01502-w
6. Adler RA. Glucocorticoid-induced osteoporosis: management challenges in older patients. *J Clin Densitom*. 2019;22(1):20–24. doi:10.1016/j.jocd.2018.03.004
7. Zhao Y, Zhou Y, Xu J, et al. Cross-kingdom RNA transport based on extracellular vesicles provides innovative tools for plant protection. *Plants*. 2024;13(19):2712. doi:10.3390/plants13192712
8. Shao M, Jin X, Chen S, Yang N, Feng G. Plant-derived extracellular vesicles-a novel clinical anti-inflammatory drug carrier worthy of investigation. *Biomed Pharmacother*. 2023;169:115904. doi:10.1016/j.biopha.2023.115904
9. Zhang F, Ganesan K, Liu Q, Chen J. A review of the pharmacological potential of *Spatholobus suberectus* Dunn on cancer. *Cells*. 2022;11(18):2885. doi:10.3390/cells11182885
10. Im N-K, Lee S-G, Lee D-S, Park P-H, Lee I-S, Jeong G-S. *Spatholobus suberectus* inhibits osteoclastogenesis and stimulates chondrogenesis. *Am J Chin Med*. 2014;42(05):1123–1138. doi:10.1142/S0192415X14500700
11. Lin WY, Dharini KK, Peng CH, et al. Zebrafish models for glucocorticoid-induced osteoporosis. *Tzu Chi Med J*. 2022;34(4):373–380. doi:10.4103/tcmj.tcmj_80_22

12. Rosa JT, Laizé V, Gavaia PJ, Cancela ML. Fish models of induced osteoporosis. *Front Cell Dev Biol*. 2021;9:672424. doi:10.3389/fcell.2021.672424
13. Zhang C, Huang R, Ma X, et al. The ribosome biogenesis factor Ltv1 is essential for digestive organ development and definitive hematopoiesis in Zebrafish. *Front Cell Dev Biol*. 2021;9:704730. doi:10.3389/fcell.2021.704730
14. Zhang C, Lu T, Zhang Y, et al. Rapid generation of maternal mutants via oocyte transgenic expression of CRISPR-Cas9 and sgRNAs in zebrafish. *Sci Adv*. 2021;7(32):eabg4243.
15. Li Z, Yu Q, Cui X, et al. Exosomes from young plasma stimulate the osteogenic differentiation and prevent osteoporosis via miR-142-5p. *Bioact Mater*. 2025;49:502–514. doi:10.1016/j.bioactmat.2025.03.012
16. Chen L, Lu L, Fan C, et al. Autophagy-induced osteoblast-derived exosomes maintain bone formation and prevent osteoporosis by remodeling gut microbiota-metabolism. *Biomed J*. 2025;49:100870. doi:10.1016/j.bj.2025.100870
17. Zhang Y, Bai J, Xiao B, Li C. BMSC-derived exosomes promote osteoporosis alleviation via M2 macrophage polarization. *Mol Med*. 2024;30(1):220. doi:10.1186/s10020-024-00904-w
18. Jangam TC, Desai SA, Patel VP, Pagare NB, Raut ND. Exosomes as therapeutic and diagnostic tools: advances, challenges, and future directions. *Cell Biochem Biophys*. 2025:1–25.
19. Rana R, Devi SN, Bhardwaj AK, Yashavarddhan M, Bohra D, Ganguly NK. Exosomes as nature's nano carriers: promising drug delivery tools and targeted therapy for glioma. *Biomed Pharmacother*. 2025;182:117754. doi:10.1016/j.biopha.2024.117754
20. Lahouty M, Fadaee M, Shanehbandi D, Kazemi T. Exosome-driven nano-immunotherapy: revolutionizing colorectal cancer treatment. *Mol Biol Rep*. 2025;52(1):83. doi:10.1007/s11033-024-10157-9
21. Jin X, Zhang J, Zhang Y, et al. Different origin-derived exosomes and their clinical advantages in cancer therapy. *Front Immunol*. 2024;15:1401852. doi:10.3389/fimmu.2024.1401852
22. Fu P, Yin S, Cheng H, Xu W, Jiang J. Engineered exosomes for drug delivery in cancer therapy: a promising approach and application. *Curr Drug Deliv*. 2024;21(6):817–827. doi:10.2174/1567201820666230712103942
23. Koh HB, Kim HJ, Kang S-W, Yoo T-H. Exosome-based drug delivery: translation from bench to clinic. *Pharmaceutics*. 2023;15(8):2042. doi:10.3390/pharmaceutics15082042
24. Mehryab F, Rabbani S, Shahhosseini S, et al. Exosomes as a next-generation drug delivery system: an update on drug loading approaches, characterization, and clinical application challenges. *Acta Biomater*. 2020;113:42–62. doi:10.1016/j.actbio.2020.06.036
25. Bian -D-D, Zhang X, Zhu X-R, et al. The Nrf2-Keap1/ARE signaling pathway in aquatic animals. *Int J Biol Macromol*. 2025;308:142595. doi:10.1016/j.ijbiomac.2025.142595
26. Wang W, Jiang H, Yu J, Lou C, Lin J. Astaxanthin-mediated Nrf2 activation ameliorates glucocorticoid-induced oxidative stress and mitochondrial dysfunction and impaired bone formation of glucocorticoid-induced osteonecrosis of the femoral head in rats. *J Orthop Surg Res*. 2024;19(1):294. doi:10.1186/s13018-024-04775-z
27. Qiu C, Li Z, Peng P. Human umbilical cord mesenchymal stem cells protect MC3T3-E1 osteoblasts from dexamethasone-induced apoptosis via induction of the Nrf2-ARE signaling pathway. *Regener Ther*. 2024;27:1–11. doi:10.1016/j.reth.2024.02.009
28. Zhang X, Pang R, Zhang K, et al. Apocynin exerts cytoprotective effects on dexamethasone-induced osteoblasts by inhibiting oxidative stress through the Nrf2 signalling pathway. *J Cell Mol Med*. 2023;27(23):3911–3927. doi:10.1111/jcmm.17974
29. Komori T. Regulation of skeletal development and maintenance by Runx2 and Sp7. *Int J Mol Sci*. 2024;25(18):10102. doi:10.3390/ijms251810102
30. Komori T. Bone development by Hedgehog and Wnt signaling, Runx2, and Sp7. *J Bone Miner Metab*. 2025;43(1):33–38. doi:10.1007/s00774-024-01551-1
31. Liu Q, Li M, Wang S, Xiao Z, Xiong Y, Wang G. Recent advances of osterix transcription factor in osteoblast differentiation and bone formation. *Front Cell Dev Biol*. 2020;8:601224. doi:10.3389/fcell.2020.601224
32. Sun X, Chen Y, Zhang Y, et al. Exosomes released from immature neurons regulate adult neural stem cell differentiation through microRNA-7a-5p. *Stem Cells*. 2025;43(2):sxae082. doi:10.1093/stmcls/sxae082
33. Yuan Y, Tan S, Wang H, et al. Mesenchymal stem cell-derived exosomal miRNA-222-3p increases Th1/Th2 ratio and promotes apoptosis of acute myeloid leukemia cells. *Anal Cell Pathol*. 2023;2023(1):4024887. doi:10.1155/2023/4024887
34. Vahidinia Z, Azami Tameh A, Barati S, Izadpanah M, Seyed Hosseini E. Nrf2 activation: a key mechanism in stem cell exosomes-mediated therapies. *Cell Mol Biol Lett*. 2024;29(1):30.
35. Liu M, Chen R, Xu Y, Zheng J, Wang M, Wang P. Exosomal miR-141-3p from PDLSCs alleviates high glucose-induced senescence of PDLSCs by activating the KEAP1-NRF2 signaling pathway. *Stem Cells Int*. 2023;2023(1):7136819. doi:10.1155/2023/7136819
36. Wang Y, Xu R, Yan Y, et al. Exosomes-mediated signaling pathway: a new direction for treatment of organ ischemia-reperfusion injury. *Biomedicines*. 2024;12(2):353. doi:10.3390/biomedicines12020353
37. Yang J, Ai X, Zhang C, Guo T, Feng N. Application of plant-derived extracellular vesicles as novel carriers in drug delivery systems: a review. *Expert Opin Drug Deliv*. 2025;22(6):787–803. doi:10.1080/17425247.2025.2487589
38. Langellotto MD, Rassu G, Serri C, Demartis S, Giunchedi P, Gavini E. Plant-derived extracellular vesicles: a synergetic combination of a drug delivery system and a source of natural bioactive compounds. *Drug Deliv Transl Res*. 2025;15(3):831–845. doi:10.1007/s13346-024-01698-4
39. Zhu Y, Zhao J, Ding H, et al. Applications of plant-derived extracellular vesicles in medicine. *MedComm*. 2024;5(10):e741. doi:10.1002/mco2.741
40. Liu Z, Guo Y, Deng Y, Shao J, Huang X, Cao Z. The potential of plant-derived vesicles in treating periodontitis and associated systemic diseases: current advances and future directions. *J Nanobiotechnol*. 2025;23(1):568. doi:10.1186/s12951-025-03651-0
41. Zhang M, Liu Y, Afzali H, Graves DT. An update on periodontal inflammation and bone loss. *Front Immunol*. 2024;15:1385436. doi:10.3389/fimmu.2024.1385436
42. Alhasan H, Terkawi MA, Matsumae G, et al. Inhibitory role of Annexin A1 in pathological bone resorption and therapeutic implications in periprosthetic osteolysis. *Nat Commun*. 2022;13(1):3919. doi:10.1038/s41467-022-31646-0
43. Mun J-G, Song D-H, Kee J-Y, Han Y. Recent advances in the isolation strategies of plant-derived exosomes and their therapeutic applications. *Curr Issues Mol Biol*. 2025;47(3):144. doi:10.3390/cimb47030144